



OPEN

Siderite-based anaerobic iron cycle driven by autotrophic thermophilic microbial consortium

Daria G. Zavarzina^{1✉}, Tatiana V. Kochetkova¹, Nataliya I. Chistyakova², Maria A. Gracheva^{2,3}, Angelina V. Antonova², Alexander Yu. Merkel¹, Anna A. Perevalova¹, Michail S. Chernov⁴, Yury A. Koksharov², Elizaveta A. Bonch-Osmolovskaya^{1,5}, Sergey N. Gavrillov¹ & Andrey Yu. Bychkov⁴

Using a sample from a terrestrial hot spring (pH 6.8, 60 °C), we enriched a thermophilic microbial consortium performing anaerobic autotrophic oxidation of hydrothermal siderite (FeCO₃), with CO₂/bicarbonate as the electron acceptor and the only carbon source, producing green rust and acetate. In order to reproduce Proterozoic environmental conditions during the deposition of banded iron formation (BIF), we incubated the microbial consortium in a bioreactor that contained an unmixed anoxic layer of siderite, perfectly mixed N₂/CO₂-saturated liquid medium and microoxic (2% O₂) headspace. Long-term incubation (56 days) led to the formation of magnetite (Fe₃O₄) instead of green rust as the main product of Fe(II) oxidation, the precipitation of newly formed metabolically induced siderite in the anoxic zone, and the deposition of hematite (Fe₂O₃) on bioreactor walls over the oxycline boundary. Acetate was the only metabolic product of CO₂/bicarbonate reduction. Thus, we have demonstrated the ability of autotrophic thermophilic microbial consortium to perform a short cycle of iron minerals transformation: siderite–magnetite–siderite, accompanied by magnetite and hematite accumulation. This cycle is believed to have driven the evolution of the early biosphere, leading to primary biomass production and deposition of the main iron mineral association of BIF.

Siderite (FeCO₃) is one of the main ferrous-containing minerals in the Earth's crust that is involved in the global cycling of iron and carbon. A significant part of existing siderite was accumulated in banded iron formations (BIF), known to be the largest source of iron ores in the world^{1–4}. These sedimentary marine rocks consisting of Fe-rich laminae (bands) containing magnetite, martite, hematite, siderite, iron silicates and, to a lesser extent, pyrite alternating with cherty Si-rich layers, formed on all continents during a period lasting from 3800 to 1800 million years ago^{4,5}. Most researchers agree that iron at the time existed in its ferrous form, and some suggest that siderite was the primary mineral in these formations^{2,5–8}. It is also generally accepted that microorganisms such as phototrophs, photoferrotrophs, nitrate-dependent iron oxidisers, and iron reducers participated in BIF deposition^{3–5,9–11}. Thus, siderite is one of the minerals that could have been directly involved in biogeochemical cycles that were functional long before the appearance of oxygen in the atmosphere^{2,5,6,8}.

Iron can serve as an energy source or electron acceptor for many prokaryotes and is the second most abundant redox-active element on Earth, after oxygen⁹. The discovery of dissimilatory iron-reducing bacteria (DIRB)^{12,13} prompted active investigation of the ability of these microorganisms to transform Fe(III)-containing minerals. Dissimilatory Fe(III)-reducing prokaryotes inhabit almost all mineral-rich anoxic environments^{14–18} and gain energy through the reduction of various Fe(III)-containing minerals, e.g. oxyhydroxides^{19,20}, clay minerals^{21,22}, and phyllosilicates²³. It is worth noting that magnetite and siderite are the main reduced minerals produced in microbial iron reduction^{14–17}.

Anaerobic microbial oxidation of ferrous iron has not been the subject of a significant amount of research. Two processes have been studied the most, photosynthetic Fe(II)-oxidation²⁴ and nitrate-dependent Fe(II)-oxidation²⁵,

¹Winogradsky Institute of Microbiology, Federal Research Centre "Fundamentals of Biotechnology", Russian Academy of Sciences, Prospekt 60 Letiya Oktyabrya 7, bld. 2, Moscow 117312, Russian Federation. ²Department of Physics, Lomonosov Moscow State University, Leninskie Gory 1, Moscow 119991, Russian Federation. ³Department of Analytical Chemistry, Institute of Chemistry, Eötvös Loránd University, Pázmány P. s. 1/A, Budapest 1117, Hungary. ⁴Department of Geology, Lomonosov Moscow State University, Leninskie Gory 1, Moscow 119991, Russian Federation. ⁵Department of Biology, Lomonosov Moscow State University, Leninskie Gory 1-12, Moscow 119991, Russian Federation. ✉email: zavarzinatwo@mail.ru

and several researchers have demonstrated the possibility of siderite oxidation in both of them^{24–26}. Both of these processes, which are thought to be involved in BIF deposition^{3,4,9–11}, would have had limited energy sources under the Precambrian conditions. Photoferrotrophs require specific surface habitats with access to both light and ferrous iron, while nitrate-dependent Fe(II)-oxidising bacteria require the presence of nitrate, which is unlikely to have been available in significant amount under the anoxic conditions of early Earth^{3,9,10}. The third, recently demonstrated route of anaerobic microbial iron oxidation has only been shown for alkaliphilic bacteria. The autotrophic Fe(III)-reducing bacterium *Geoalkalibacter ferrihydriticus* was shown to be capable of transforming biotite and glauconite, Fe(II)/Fe(III)-containing phyllosilicates, to magnetite in the presence of acetate at pH 9.5¹⁷. During the experiment, the additional formation of acetate was observed instead of its expected oxidation, while Mössbauer spectral analysis revealed that magnetite was formed due to Fe(II)-oxidation rather than Fe(III)-reduction. Based on these observations, we hypothesize that this microorganism would be able to perform carbonate-dependent Fe(II)-oxidation. Thermodynamic calculations supported this suggestion¹⁷. Further investigations demonstrated the ability of alkaliphilic autotrophic acetogenic bacterium *Fuchsiella ferrireducens*, as well as a syntrophic culture of *G. ferrihydriticus* and *Candidatus* “Contubernalis alkalaceticum” to oxidise siderite anaerobically in the presence of ethanol^{27,28}.

Genomic reconstruction of the last universal common ancestor (LUCA) metabolism performed by Weiss et al. revealed that LUCA was probably an anaerobic, CO₂-fixing, H₂-dependent and N₂-fixing thermophilic microorganism capable of performing the Wood–Ljungdahl pathway²⁹. On the other hand, extracellular electron transfer (EET), including processes driving anaerobic reduction and oxidation of iron minerals, are thought to have been amongst the first respiratory pathways that appeared on the hot early Earth³⁰. Thus, carbonate-dependent iron oxidation by thermophilic microorganisms may have played a significant role in the early development of Earth biosphere.

The main goal of the present research was to demonstrate the capability of a thermophilic microbial consortium to perform autotrophic anaerobic oxidation of hydrothermal siderite. Cultivating the consortium in a bioreactor with a microoxic headspace, simulating the conditions of early/mid Proterozoic ocean, we were able to assess the possible contribution of this process to BIF accumulation.

Results

Obtaining a stable anaerobic thermophilic siderite-oxidising microbial consortium. We obtained the primary enrichment culture from a sediment/water sample of the Solnechny hot spring (“Sun spring”, the Uzon Caldera, Kamchatka Peninsula, Russia), which has a temperature of 60 °C and pH of 6.8. A stable siderite-oxidising anaerobic thermophilic microbial consortium was obtained by ten-fold dilutions and multiple consequent transfers (see “Methods”) on bicarbonate medium with hydrothermal siderite as the electron donor and 20% of CO₂ in the gas phase as the electron acceptor. After ten days of incubation, the population density had reached 5 × 10⁶ cell ml⁻¹ and up to 0.5 mM acetate had formed. The initial siderite had been transformed into a grey precipitate (Supplementary Fig. S1) and thin mineral lamellae of green-brownish colour. The new mineral phase was identified by Mössbauer spectroscopy as green rust, FeCO₃ × 3Fe(OH)₂ × 2Fe(OH)₃ × 2H₂O (Supplementary Fig. S2a,b; Supplementary Table S1). A Mössbauer spectrum of the sterile control showed no changes in the initial mineral phase of hydrothermal siderite (Supplementary Fig. S2c,d). Using scanning electron microscopy (SEM), thin spherical crystals of green rust were found on the surface of hydrothermal siderite particles. In addition, dense sphere-shaped particles with an average size of 2–5 μm were observed to precipitate separately (Supplementary Fig. S3b,c). The lamellae, with thickness ranging from 15 to 20 μm, consisted of tabular crystals of green rust arranged in mutually perpendicular orientation (Supplementary Fig. S3d–f).

The analysis of microbial abundance and diversity in the siderite-oxidising consortium, based on the high throughput sequencing and counting of 16S ribosomal ribonucleic acid (rRNA) gene amplicons, showed predominance of Gram-positive bacteria of the genus *Carboxydotherrmus* (69% of the total community). The rest of operational taxonomic units (OTUs) belonged to the genera *Fervidobacterium* (11%), *Thermanaerothrix* (6%), *Thermodesulfovibrio* (4%), *Thermoanaerobaculum* and *Paludibaculum* (1% total) (Supplementary Fig. S4).

Scaling up the anaerobic siderite-oxidising microbial consortium. In order to reproduce possible processes of biogeochemical siderite transformation in Proterozoic environments, the enriched microbial consortium was incubated in a bioreactor. The reactor was set up in a mixing regime that allowed for the separation of three different phases: an unmixed hydrothermal siderite layer at the bottom of the reactor; a water column intermittently bubbled with N₂/CO₂ (80/20) gas mixture to saturation; and headspace gas (15% of the total volume) composed of N₂/CO₂/O₂ (78/20/2 v/v). Gas outflow was controlled to prevent both air entrapment and unwanted rise in the amount of dissolved CO₂ due to overpressure. The experiment lasted 56 days.

Unlike with the initial culture, no change of siderite colour was observed in the bioreactor-grown consortium during the course of the experiment. Mössbauer spectroscopic monitoring of siderite transformation revealed a new doublet, steadily increasing over the course of incubation, that was identified as newly formed siderite (Fig. 1a, Table 1, Supplementary Fig. S5, Supplementary Table S2). X-ray powder diffraction analysis (XRD) of a mineral sample taken at the end of the experiment (Supplementary Fig. S6) revealed the presence of the initial hydrothermal siderite (lattice parameters: $a = 4.684 \pm 0.001$ Å, $c = 15.386 \pm 0.001$ Å) and newly formed siderite ($a = 4.701 \pm 0.001$ Å, $c = 15.407 \pm 0.005$ Å), thus confirming the results of Mössbauer spectroscopic analysis. In addition to the new doublet, Mössbauer spectra revealed a sextet which was present almost constantly throughout the experiment and could be attributed to a magnetically ordered phase (Fig. 1a, Table 1, Supplementary Fig. S5). Based on its parameters, this magnetically ordered phase was identified as magnetite (Supplementary Table S2). The presence of magnetite was supported by the electron paramagnetic resonance (EPR) spectral characteristics of experimental and control mineral samples determined at the end of incubation. A considerable signal of the

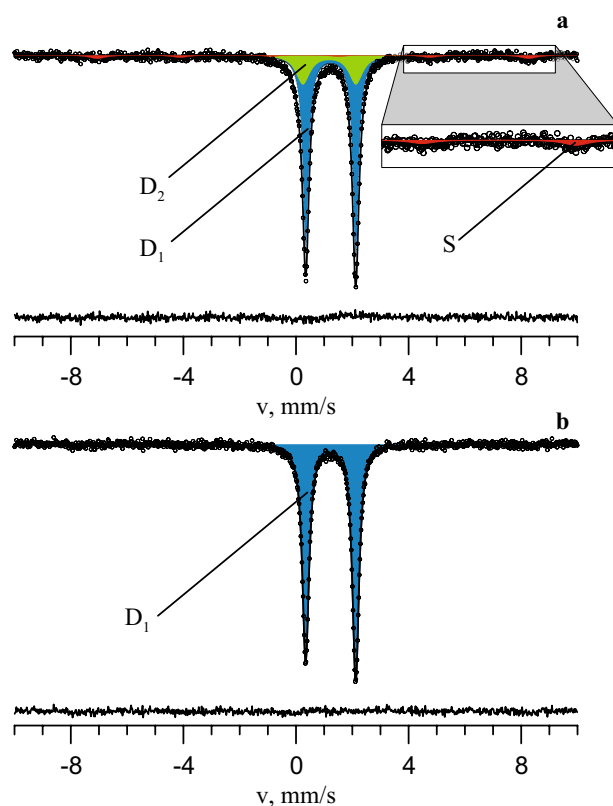


Figure 1. Mössbauer spectrum measured at room temperature of the mineral phase sampled from the bioreactor culture (a) and sterile control (b) on the 56th day of incubation. D₁ corresponds to Fe²⁺ ions in the structure of initial siderite, D₂—to Fe²⁺ ions in the structure of biogenic siderite, S—to magnetically ordered phase.

Day	Cell density, cells/ml	Phylogenetic composition of the microbial consortium, %	Acetate, mM	Mineral phase composition, %
0	3.0×10^5	<i>Carboxydotherrmus</i> (69), <i>Fervidobacterium</i> (11), <i>Thermanaerotherrix</i> (6), <i>Thermodesulfovibrio</i> (4), <i>Thermoanaerobaculum</i> (1), <i>Paludibaculum</i> (0.3), <i>Chthonomonadales</i> (0.07)	0	HS (100)
7	1.0×10^7	ND	0.01	HS (100)
14	1.1×10^7	<i>Carboxydotherrmus</i> (5), <i>Fervidobacterium</i> (0.5), <i>Thermanaerotherrix</i> (90), <i>Thermodesulfovibrio</i> (2), <i>Thermoanaerobaculum</i> (0.7), <i>Paludibaculum</i> (1), <i>Chthonomonadales</i> (0.06)	0.06	HS (91) MIS (5), M (4)
21	0.9×10^7	ND	ND	HS (90), MIS (6), M (4)
28	1.9×10^7	<i>Carboxydotherrmus</i> (0.1), <i>Fervidobacterium</i> (0.04), <i>Thermanaerotherrix</i> (98), <i>Thermodesulfovibrio</i> (0.5), <i>Thermoanaerobaculum</i> (0.09), <i>Paludibaculum</i> (0.5), <i>Chthonomonadales</i> (0.1)	0.12	HS (80), MIS (13), M (7)
35	2.5×10^7	ND	ND	HS (79), MIS (15), M (6)
42	7.6×10^7	<i>Carboxydotherrmus</i> (0.3), <i>Fervidobacterium</i> (0.5), <i>Thermanaerotherrix</i> (80), <i>Thermodesulfovibrio</i> (9), <i>Thermoanaerobaculum</i> (0.1), <i>Paludibaculum</i> (5), <i>Chthonomonadales</i> (4), <i>Thermaerobacter</i> (2)	0.21	HS (79), MIS (17), M (4)
49	2.6×10^7	ND	0.09	HS (75), MIS (18), M (7)
56	0.9×10^7	<i>Carboxydotherrmus</i> (0.2), <i>Fervidobacterium</i> (0.5), <i>Thermanaerotherrix</i> (79), <i>Thermodesulfovibrio</i> (7), <i>Thermoanaerobaculum</i> (0.5), <i>Paludibaculum</i> (6), <i>Chthonomonadales</i> (4), <i>Thermaerobacter</i> (3)	0.1	HS (70), MIS (23), M (7)

Table 1. Summarized parameters of the bioreactor culture for the 56-day incubation period. HS, hydrothermal siderite; MIS, metabolically induced siderite; M, magnetite; ND, not determined.

magnetic material was observed in the spectra of the experimental samples (Supplementary Fig. S7). Its width was about 1300 Oe and the g-factor was equal to 2.3, supporting that the sample contained magnetite, probably, in the form of nanoparticles³¹.

E_h readings performed in the middle part of water column during the long-term incubation fluctuated from -7 to -109 mV [vs standard hydrogen electrode (SHE)] indicating anaerobic conditions. During short periods of active mixing of the culture prior to each sampling (see “Methods” section), mineral particles rose to the top part of the bioreactor and precipitated onto its glass walls and rotating shaft. The bottom edge of the precipitate,

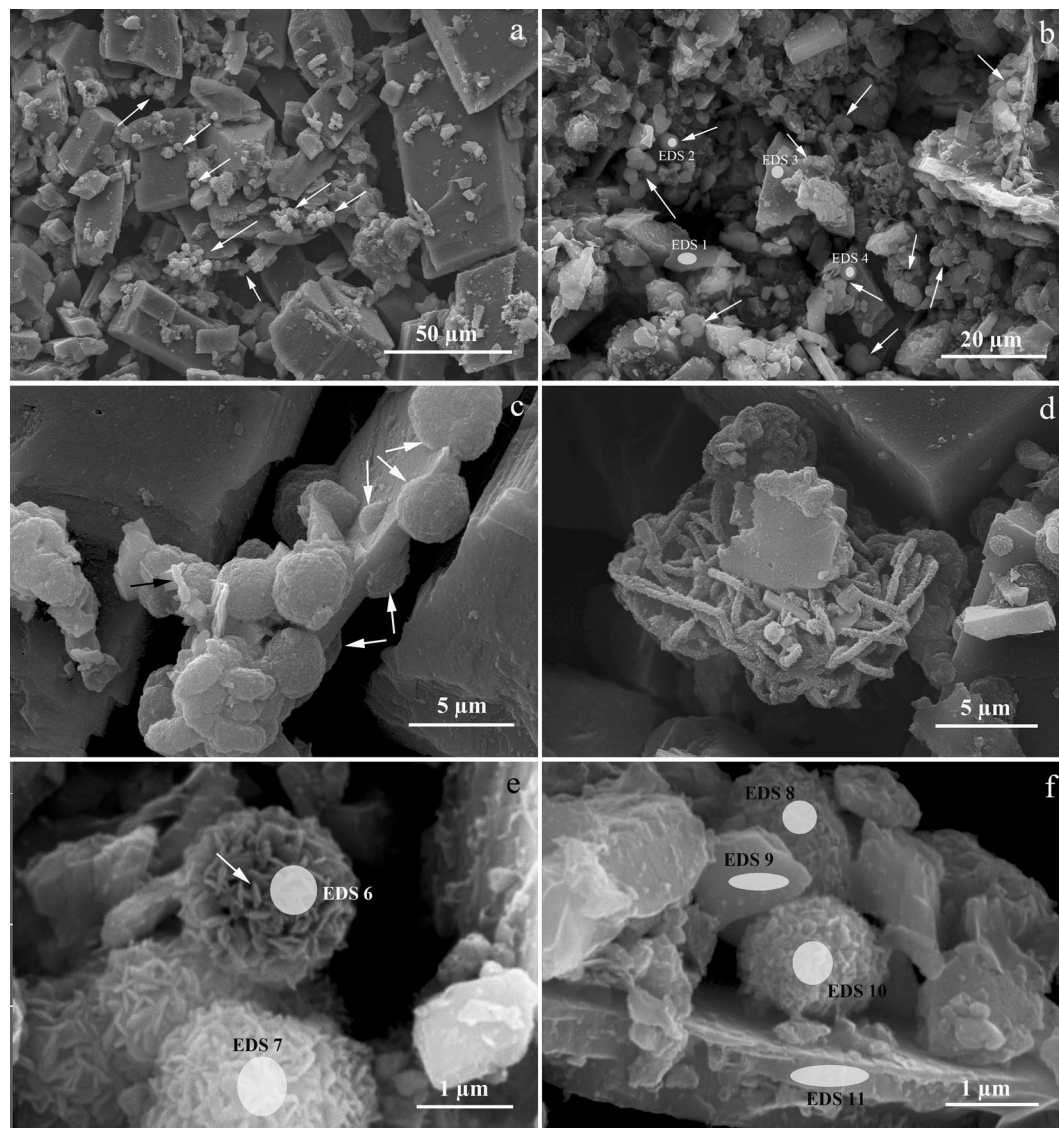


Figure 2. SEM micrographs of the mineral phase (bioreactor culture) sampled after the end of the experiment: (a) general view of hydrothermal siderite particles with newly formed globules pointed by white arrows; (b) hydrothermal siderite and newly formed globules (white arrows); spots of EDS analysis (white ovals) (Supplementary Table S4); (c) metabolically induced siderite globules formed on the surface of hydrothermal siderite (white arrows) and bacterial cells (black arrow); (d) fossilized bacterial cells; (e,f) structure of globules consisting of small flat crystals. White ovals indicate spots of EDS analysis (Supplementary Table S4).

as well as the results of an independent E_h measurement in the upper part of the liquid medium column at the end of incubation (+30 mV vs SHE), indicated oxycline (Supplementary Fig. S8). This mineral precipitate was analysed using Mössbauer spectroscopy and was found to consist of a mixture of hydrothermal siderite and newly formed phases: hematite micro-particles ($18.9 \pm 0.6\%$), green rust ($17.5 \pm 2.8\%$), and an unidentified phase containing Fe(III) ($10.6 \pm 0.5\%$) (Supplementary Fig. S9; Supplementary Table S3). No changes in the initial mineral phase of siderite were observed by Mössbauer spectroscopy in concurrently incubated sterile controls (Fig. 1b) despite of 2% O_2 present in their headspace. No soluble or HCl-extractable ferrous or ferric iron species were detected colorimetrically in the bioreactor culture or the control at any time during the incubation. The pH of the bioreactor culture was sustained automatically, and no changes in the pH of both culture and uninoculated control were detected during incubation, indicating that iron speciation in the studied media was not influenced by changes in proton activity.

At the end of the experiment, SEM revealed abundant spherical-shaped particles in the mineral phase of the bioreactor (globules Fig. 2a,b), with an average size of about 2–5 μm , typical of previously reported metabolically induced siderite³². Some globules were formed on the surface of the initial hydrothermal siderite particles (Fig. 2c). Mineral nanoparticles encrusting bacterial cells were also observed (Fig. 2c,d). The globules consisted of small nanometric-size, slightly curved flat crystals (Fig. 2e,f). Energy dispersive X-ray spectroscopy (EDS)

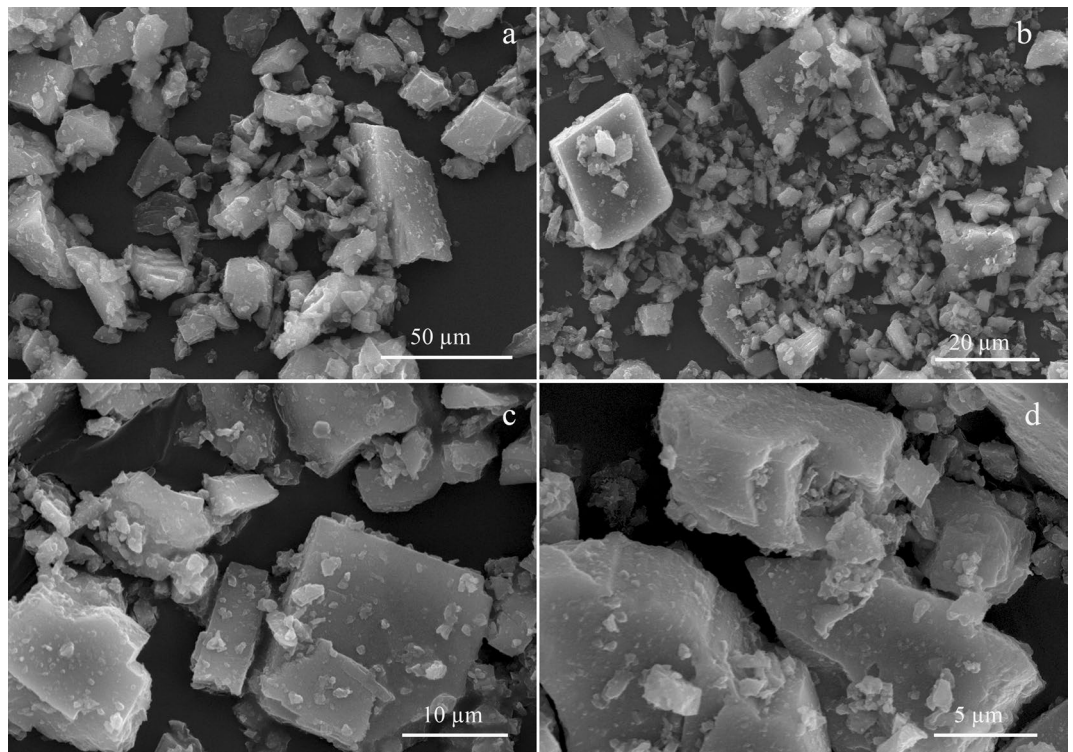


Figure 3. SEM micrographs of hydrothermal siderite particles from sterile control after the end of incubation at different (a–d) magnifications.

revealed that the elemental composition of the newly formed globules was identical to that of the particles of hydrothermal siderite and, thus, supported the data from the Mössbauer spectroscopy and XRD. The only significant difference in elemental composition of the hydrothermal siderite and globules was the increased content of phosphorus in the globules that indicated their biogenic origin (Fig. 2b,e,f; Supplementary Table S4). SEM/EDS studies revealed no significant changes of hydrothermal siderite in sterile control (Fig. 3).

16S rRNA gene fragment analysis showed the predominance of bacteria of the genus *Thermanaerotherix* in the bioreactor from the 25th day of incubation until the end of the experiment (Table 1). Total cell density increased from 3.0×10^5 to 1.0×10^7 cell ml^{-1} by the 7th day of the experiment and then varied only slightly, as did the acetate concentration (Table 1).

Total organic carbon (TOC) content in the mineral phases was analysed using Rock–Eval pyrolysis method³³ at the end of incubation and was twenty times higher in the experimental sample than in the control (0.043 versus 0.002 wt%) (Supplementary Table S5). This result clearly indicated active carbon assimilation by the microbial consortium during its growth in the bioreactor.

Discussion

Thermophilic prokaryotes are believed to originate around 3.8 billion years ago, when the Earth surface had cooled down enough for stable atmosphere and ocean to form; however, ocean temperatures were still elevated, ranging from 55 to 80 °C³⁴. A wide variety of thermophilic bacteria and archaea inhabit modern thermal environments, many of which (especially those of volcanic origin) retain physical and chemical conditions of early Earth. For our experiments, we chose a terrestrial hot spring Solnechny in the Uzon Caldera (Kamchatka volcanic belt), previously shown to have a highly diverse microbial community and visible deposition of iron minerals³⁵. Using the ten-fold dilution method and consequent transfers on the medium with hydrothermal siderite as a sole electron donor, we obtained a consortium of thermophilic bacteria able to derive energy from iron redox transformation (Supplementary Fig. S4). Bacteria of the genus *Carboxydotherrmus*, which were present in the enrichment are perfect candidates for performing carbonate-dependent iron oxidation, as some of them possess both the Wood–Ljungdahl and EET pathways^{36–38}. Species of other genera, e.g., *Thermodesulfovibrio*, *Thermoanaerobaculum* and *Paludibaculum*, are capable of iron reduction^{39–41}. The ability of these organisms to carry out anaerobic Fe(II) oxidation has never been tested. However, the proposed phylogenetic relations between Fe(III)-reducing and Fe(II)-oxidising EET pathways^{38,42} as well as the demonstration of the ability of *G. ferrireducens* and *F. ferrireducens* to reduce and oxidise iron minerals under anoxic conditions^{17,27,32} support such a possibility.

Mössbauer spectroscopy identified green rust, which is a mixed-valent Fe(II)–Fe(III) hydroxycarbonate, as the sole product of microbial siderite transformation by the initial consortium. Usually, green rust is an intermediate product of aerobic oxidation of ferrous hydroxide, anaerobic iron transformation in hydromorphic soils⁴³ or anaerobic ferric oxihydroxides and magnetite reduction by DIRB⁴¹. On these grounds, green rust is assumed to play an important role in the biogeochemical cycle of iron; it could be found under environmental conditions that

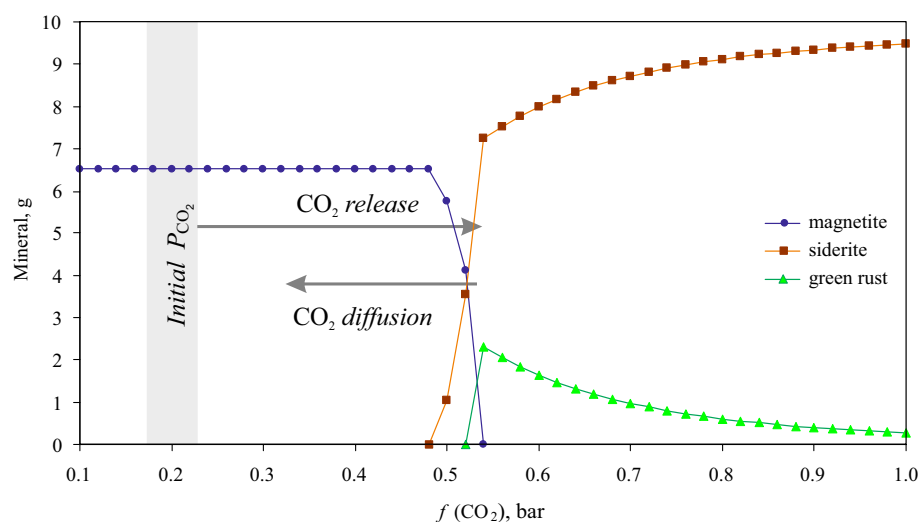
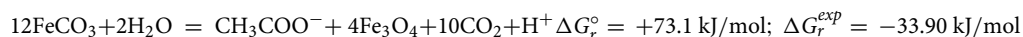


Figure 4. Thermodynamic calculations of equilibrium mineral associations at $f(\text{CO}_2)$ from 0.1 to 1.0 bar made for experimental conditions. Initial CO_2 fugacity (0.2 bar) changes in the layer of siderite which is not stable. Carbon dioxide released by reaction (1) can induce a local increase of CO_2 . At a carbon dioxide fugacity more than 0.52 bar siderite becomes stable again.

equally favour biogenic iron oxidation and iron reduction⁴⁵. In addition to green rust, SEM analysis revealed the formation of new spherical particles (Supplementary Fig. S3b,c) which we assumed to represent a metabolically induced siderite. However, the Mössbauer spectra of siderite and subspectra of Fe(II)-positions in green rust are too similar for these minerals to be distinguished.

The incubation of the siderite-oxidising microbial consortium in a bioreactor with two different mixing modes and 2% O_2 in the headspace was designed to simulate Proterozoic environmental conditions⁴⁶. This experiment confirmed biogenic redox cycling from hydrothermal to metabolically induced siderite, proposed to occur in the initial enrichment. The conditions reproduced in the bioreactor, specifically the maintenance of a constant CO_2 concentration in the liquid medium and the presence of a microoxic zone near the gas-to-liquid interface, significantly influenced both the phylogenetic composition of the consortium (Table 1) and the products of siderite transformation (Figs. 1, 2; Table 1; Supplementary Fig. S5; Supplementary Table S2). For example, bacteria of the genus *Thermaerobacter* capable of aerobic growth appeared amongst the obligate anaerobes.

Two new mineral phases, magnetite and newly formed siderite, were detected in the unmixed mineral phase of the bioreactor culture by Mössbauer and EPR spectroscopy, XRD and SEM/EDS. Thermodynamic calculations of the Gibbs free energy changes for the conditions of the experiment ($T = 60^\circ\text{C}$, $\text{pH} = 6.8$, $f(\text{CO}_2) = 0.2$ bar, $[\text{Ac}] = 0.001$ mol) revealed that siderite is unstable and could be oxidised by anaerobic thermophiles through the following reaction:



The equilibrium value of the CO_2 fugacity (0.52 bar) allowed the coexistence of siderite and magnetite but restricted further oxidation. At higher CO_2 fugacity, magnetite becomes unstable (Fig. 4). Carbon dioxide released in this reaction (1) can induce a local increase in CO_2 fugacity inside the unmixed mineral sediment and, by doing so, initiate a reverse reaction of magnetite reduction to siderite. This reverse reaction can be performed by the organotrophic iron-reducing microorganisms present in the consortium, in particular those of the genera *Carboxydotherrmus*, *Thermodesulfovibrio*, *Thermoanaerobaculum* or *Paludibaculum*, which could use newly formed acetate or biomass of autotrophs as the electron donor. The newly formed siderite in the bioreactor crystallised in the form of spherical aggregates identical to those we observed in the enrichment culture (Supplementary Fig. S2c) and was quite different from the original hydrothermal siderite particles (Figs. 2, 3). Such a morphology is fairly common for sedimentary siderite precipitated from saturated solutions⁸, in the reaction of glucose with ferrihydrite at pressure and temperature typical to diagenesis³, or formed by dissimilatory iron reducers^{14,32,47}. Moreover, the parameters of Mössbauer spectra of siderite obtained in our experiments were identical to those reported previously for siderite produced by the thermophilic bacterium *Thermincola ferriacetica* in the course of ferrihydrite reduction⁴⁸. Given these facts and the thermodynamic calculations, we propose the formation of metabolically induced siderite as the most probable process closing the iron cycle performed by the thermophilic microbial consortium (Fig. 5). The content of the newly formed siderite increased during the incubation, while the relative content of magnetite remained practically constant (Table 1; Supplementary Fig. S5), meaning the microbial consortium acted as a conveyor transforming hydrothermal siderite to new siderite with magnetite and acetate as intermediate products. The diffusion rate of carbon dioxide in the mineral and liquid phases and the metastability of siderite seems to serve as the master switch of this cycle, turning on or off the formation of magnetite (Fig. 5).

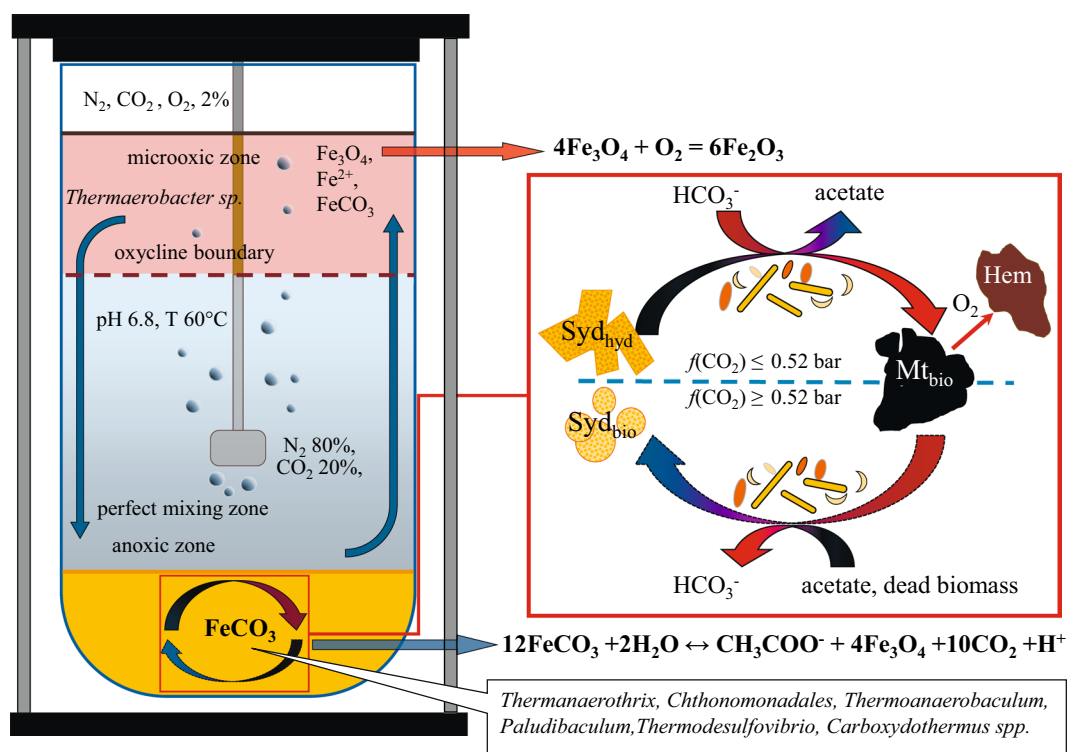


Figure 5. Schematic representation of the proposed processes in the bioreactor culture. *Sid_{hyd}* hydrothermal siderite, *Sid_{bio}* metabolically induced siderite, *Mt_{bio}* metabolically induced magnetite, *Hem* hematite, red square anaerobic iron cycle driven by the thermophilic microbial consortium at the bottom of the bioreactor (in the mineral sludge).

The precipitation of hematite that occurred in the upper part of the bioreactor at the water–gas interface (Supplementary Fig. S8) was caused by oxidation of magnetite and siderite particles uplifted to the microoxic zone of the bioreactor during the sampling procedure (Fig. 5). Hematite, is a thermodynamically stable phase, accumulated as a secondary mineral during the experiment and, most likely, did not participate in the iron cycle driven by the anaerobic microbial consortium due to its low bioavailability as electron acceptor^{19,49}.

The anaerobic microbial cycle described here has important geological implications for the period of BIF deposition. In contrast to photoferrothrophic or nitrate-dependent Fe(II)-oxidising processes, it is not limited by the availability of electron acceptors. It is widely recognised that the primary source of iron minerals in BIF was ferrous iron carried by hydrothermal fluid^{5–8} and that the CO₂ partial pressure and carbonate content never dropped below their modern levels throughout the Earth's geological history⁵⁰. Thus, the presumed conditions of early Earth could favour the evolution of anaerobic Fe(II)-oxidising microorganisms, which can use CO₂ as the only electron acceptor and carbon source via acetogenesis which was considered to be the most ancient pathway^{34,51}. In our experiments, the selected microbial consortium was able to grow without allochthonous organic matter by utilising the energy of siderite oxidation, with CO₂ as the electron acceptor and acetate as the reduced product. The rate of siderite transformation calculated from Mössbauer data (Table 1) was high: 0.5% hydrothermal siderite per day was transformed into magnetite, hematite and metabolically induced siderite. The organic matter produced in this process, i.e., acetate and cell biomass, served as the electron donors for the iron reducers, thus making further biogenic transformation of magnetite possible. The cycle resulted in the accumulation of organic matter [HAWK analysis indicated accumulation of 123 mg TOC (Supplementary Table S5)] and of a mixture of oxidised iron minerals, magnetite and secondarily formed hematite. Such a light- and oxygen-independent biological cycle of iron—from siderite to novel siderite—could have served as the driving force in the ancient biosphere, much like the cycle of oxygen (i.e., photosynthesis and respiration reactions) has served as the central biogeochemical driving force for major processes in the biosphere since the Great Oxygenation Event. Notably, the anaerobic biogeochemical iron cycle could also play a significant role in certain parts of the modern biosphere—in deep subsurface and other extreme environments devoid of light and oxygen or its derivatives but rich in redox-active iron minerals.

Conclusions

Our experiments clearly show the capability of an autotrophic thermophilic microbial consortium to perform anaerobic oxidation of hydrothermal siderite. We demonstrate that the process of anaerobic iron oxidation coupled with acetate production, which has been previously shown for alkaliphiles^{17,27,28}, is likely to have wider distribution and could be performed by microbial communities inhabiting pH-neutral thermal environments.

Thermodynamic calculations performed for our experimental conditions confirm that the communities of thermophilic bacteria can gain energy in the course of a short cycle of iron minerals redox transformations, utilising CO₂ as the electron acceptor and the primary carbon source. Growth of thermophilic bacteria based on two low-energy reactions of siderite oxidation and magnetite reduction makes the fugacity of CO₂ a master switch of this short iron cycle, either favouring, or hampering magnetite formation.

The described iron cycle sustains primary biomass production from CO₂ by chemosynthesis, thus representing one of the processes that could drive biogeochemical cycles of carbon and iron in the early Earth's biosphere as well as in modern deep subsurface biosphere. The main benefit of this process in comparison with previously known mechanisms of microbial anaerobic iron oxidation is that the process is not limited by the availability of electron donors and acceptors. The high availability of both reduced iron and CO₂ compensate for the low energy efficiency of carbonate-dependent siderite oxidation and facilitate magnetite reduction, making these reactions possible driving forces in the ancient biosphere.

The accumulation of the main BIF iron mineral association, i.e. hematite, magnetite and metabolically induced siderite, could arise from the difference in microbial siderite oxidation and magnetite reduction rates as well as from the low hematite bioavailability.

Materials and methods

Characteristic of the sampling site, sampling and obtaining of the enrichment culture. Samples of water and sediment were taken from the Solnechny (Sun) hot spring in the Uzon Caldera (54° 29.5632 N/159° 59.3164 E, 52 °C, pH 6.1), Kamchatka Peninsula, Russia, in 2015. The spring discharges at the bottom of a thermally heated swamp. The bottom of the spring is shaped like a funnel, is covered with a layer of red to orange Fe-containing deposits and is characterized by active CO₂ emanations from the central hole³⁵. The temperature and pH levels in the spring have remained fairly stable over several years of observations; the E_h value is negative and comprises – 34 mV (vs standard hydrogen electrode, SHE) at a depth of 0.5 m and around zero on the water surface where it is influenced by atmospheric precipitations. The sample was taken at a depth of 10 m below the sediment surface and transported to the laboratory in sterile anaerobic 50 ml flasks.

Characteristics of siderite. Selected grains of hydrothermal siderite FeCO₃ (Bakal deposit, Ural, Russia) were crushed into powder (< 100 µm particle size) in an agate mortar. The purity of the siderite was confirmed by X-ray diffraction that revealed no detectable impurities from secondary minerals (Supplementary Fig. S6). The absence of Fe(III) in siderite was confirmed by Mössbauer spectroscopy.

Cultivation techniques. The standard anaerobic modified Pfennig medium (mP) was used for the enrichment (g l⁻¹): 0.33 KCl, 0.33 MgCl₂ × 6H₂O, 0.11 CaCl₂, 0.33 NH₄Cl, 0.33 KH₂PO₄. After boiling, the medium was cooled under a flow of N₂/CO₂ (80/20 v/v) and simultaneously supplied with 0.7 g l⁻¹ of NaHCO₃, 1 ml l⁻¹ of trace element solution, 1 ml l⁻¹ of vitamin solution²³. The sediment and water samples from the Solnechny hot spring (2 ml) were added to the 30 ml of medium that contained 10 g l⁻¹ of hydrothermal siderite powder, and the mixture incubated in 50-ml flasks under N₂/CO₂ (80:20, v/v) at 60 °C and pH 6.8–7.0. The resulting enrichment culture was transferred (5% v/v) to a fresh medium each time the colour of the mineral phase changed from orange to grey. After five transfers, the enrichment was further processed in Hungate tubes using the tenfold dilution method, and the last positive dilution (10⁻⁶) was transferred into 50-ml flasks five times more. Control flasks were not inoculated but were incubated at the same conditions.

A stable, anaerobic thermophilic consortium that was actively transforming hydrothermal siderite, was transferred into a bioreactor set up to simulate Proterozoic environmental conditions: 180 ml inoculum (6% v/v) was anaerobically transferred to a benchtop bioreactor Labfors 4 (Infors HT, Switzerland) pre-filled with 3 L sterile medium and 300 g hydrothermal siderite powder. The bioreactor was started in batch mode with the temperature and pH controlled, and incubation was carried out over 56 days using the following mixing regime: the bottom of the reactor, a layer of a solid mineral phase (ca. 300 ml volume) was left almost unstirred. The water column over the solid phase was intermittently bubbled with a N₂/CO₂ gas mixture (80/20 v/v) and subjected to an exact mixing model with Rushton impellers mounted to the middle of the shaft operated at 50 rpm. Over the water column, a small gas headspace (0.6 l), containing a N₂/CO₂/O₂ gas mixture (78/20/2% v/v), was left with a controlled gas outflow in order to prevent gas overpressure. The volumetric ratio between the solid, liquid and gas phases of the bioreactor culture was ca. 1:9:2 (v/v). To monitor microbial growth, acetate production and siderite transformation, subsamples were taken every 7 days during the incubation period. Before each sampling, the impellers were set to 450 rpm for 30 min to provide uniform distribution of the culture components throughout its volume. Outflow gas was regularly sampled and analysed via a flow-through autosampler of a gas chromatograph (see below) connected to the exit gas cooler of the bioreactor by oxygen-tight tubing.

Uninoculated controls were incubated under the same conditions for the same duration of time in 0.5 l bottles with the same mineral/liquid/gas phases volumetric ratio (1:9:2). Sampling of gas and liquid phases was performed at the same intervals after the control bottles were thoroughly shaken by hand.

Analytical methods. Microbial growth was monitored by direct cell counting with a phase contrast light microscope (Olympus CX41RE, Japan). Possible organic products of growth (volatile fatty acids and alcohols) were assayed using a Stayer HPLC chromatograph (Aquilon, Russia), as described previously¹⁶. The gas phase was analysed using a '3700' custom-modified gas chromatograph (ZIOC RAS Special Design Tech. Dept., Russia), as described previously²³.

pH and E_h parameters of the bioreactor culture were monitored automatically using combination electrodes 405 and Pt4805, respectively (type DPAS-SC-K8S/325 by Mettler Toledo), with adjustable immersion depth. For

routine monitoring, both electrode tips were immersed down to the middle of the culture's water column. At the end of incubation, the Redox electrode was lifted to the top layer of the culture to reveal the proposed oxycline boundary zone. pH and E_h parameters of the cultures and controls that were incubated in flasks were measured in subsamples taken aseptically immediately after their collection, using a Seven2Go Pro pH/mV portable meter equipped with InLab series pH and Redox combination electrodes (all from Mettler Toledo).

Soluble and HCl-extractable iron species were determined from culture subsamples taken in diluted (0.6 N) HCl. Insoluble material was separated from HCl extracts by centrifugation at 12 kg for 10 min on an Eppendorf table top centrifuge. Clean extract was further processed for colorimetric detection of Fe^{2+} with ferrozine and Fe^{3+} with potassium thiocyanate, as previously described⁵².

The morphology of mineral samples was examined by SEM using a TESCAN VEGA 3 LMU device with an INCA Energy 350/X-max 80 energy-dispersive (EDS) analysis system (OXFORD Instruments NanoAnalysis, UK). Patterns were pre-fixed with double-sided carbon tape and triply coated with Au.

Mineral compositions were determined by X-ray diffraction analysis on a Panalytical Empyrean diffractometer using a copper anode ($\lambda = 1.54 \text{ \AA}$, $I = 40 \text{ mA}$, $U = 40 \text{ kV}$).

The $\text{Fe}^{2+}/\text{Fe}^{3+}$ ratio was determined by ^{57}Fe Mössbauer spectroscopy. This method allows for the determination and quantification of different atomic environments, magnetic states, chemical states and transformations of iron-containing compounds⁵³. All Mössbauer measurements were carried out at room temperature using an MS-1101 Em spectrometer operating in the constant acceleration mode, with ^{57}Co source in Rh matrix. To reduce the texture effect, Mössbauer measurements were performed at the "magic angle" (the absorber placed at an angle $\vartheta = 54.74^\circ$ to γ -ray direction) by placing the siderite powder samples in a paraffin cone. The calibration was constructed relative to α -Fe, and spectra were fitted with SpectrRelax software⁵⁴. When the relative content of magnetite was low, sextets that correspond to iron atoms in the A and B positions of magnetite are not resolved. In this case, a model consisting of one sextet with broadened lines with hyperfine parameters equal to the average values of parameters typical for iron atoms in the A and B positions was used for spectrum processing.

E-4 spectrometer (9.2 GHz, Varian) was used to measure the EPR at room temperature. Small grains of siderite powder samples were placed at the bottom of a narrow quartz ampoule and fixed by paraffin. The spectra were recorded using a modulation frequency of 100 kHz and microwave power of 10 mW.

For the identification of organic carbon in control and experimental siderite samples, Rock-Eval pyrolysis method³³ on HAWK Resource Workstation (Wildcat Technologies, USA) were used. The main measured organic parameters were S1 (free oil)—the amount of thermally freed hydrocarbons ($\text{C}_8 \div \text{C}_{15+}$) in the sample obtained after heating the sample to 300°C ; S2 (kerogen yield)—the amount of hydrocarbons generated through thermal ($300 \div 650^\circ\text{C}$, heating $25^\circ\text{C min}^{-1}$) cracking of non-volatile organic matter (kerogen); and S3 (organic carbon dioxide yield)—the amount of CO_2 produced during pyrolysis of kerogen, corresponding to the organic carbon dioxide yield of the rock and measured by infrared (IR) cell. TOC (wt. %) was calculated as described previously³³ based on the measured parameters.

16S rRNA gene amplification and sequencing. After the culture samples were subjected to cell disruption by bead-beater and proteinase K treatment, DNA was extracted by routine phenol–chloroform method with ethanol precipitation. The V3–V4 region of 16S rRNA genes were amplified and libraries were prepared as previously described⁵⁵. Sequencing of the libraries was performed with Illumina MiSeq platform using MiSeq Reagent Kit v3 (600 cycles). Most of the data analysis, including quality trimming, demultiplexing, taxonomic assignments and core diversity analyses were performed with QIIME⁵⁶ and SILVA online data analysis service⁵⁷. All sequencing data were entered into NCBI BioProject PRJNA626446. Basic statistics of the results obtained from the sequencing of the V3–V4 regions of the 16S rRNA gene are presented in the Supplementary Table S6.

Thermodynamic calculations. Equilibrium state calculations for the system (H–C–O–Na–Fe) were carried out using the HCh software^{58,59}. To calculate the equilibrium state, the minimum free energy of the system was determined. The thermodynamic model was analysed to determine the proportions of the phases in the experiment at a variable CO_2 partial pressure. These calculations show phase associations and solution compositions that correspond to thermodynamic equilibrium. It should be noted that such equilibrium was not reached during the experiment. The calculations were used to determine in which direction processes were moving.

Changes in Gibbs free energy of reactions were calculated using the HCh software, and the thermodynamic properties of components were taken from the Unitherm database⁵⁹. The values for the standard state (ΔG°) were recalculated for real pH values, and bicarbonate activity and free energy for reactions with experimental component activities (ΔG_r) were received. These values can be used to determine the direction of the process. Thermodynamic properties for green rust with composition $\text{FeCO}_3 \times 3\text{Fe}(\text{OH})_2 \times 2\text{Fe}(\text{OH})_3 \times 2\text{H}_2\text{O}$ were taken from Drissi et al.⁶⁰.

Received: 5 June 2020; Accepted: 27 November 2020

Published online: 10 December 2020

References

1. Kholodov, V. N. & Butuzova, G. Y. Siderite formation and evolution of sedimentary iron ore deposition in the Earth's history. *Geol. Ore Depos.* **50**, 299–319 (2008).
2. Kholodov, V. N. & Butuzova, G. Y. Problems of siderite formation and iron ore Epochs: Communication 1. Types of siderite-bearing iron ore deposits. *Lithol. Miner. Resour.* **39**, 389–411 (2004).
3. Köehler, I., Konhäuser, K. & Kappler, A. Role of microorganisms in banded iron formations. In *Geomicrobiology: Molecular and Environmental Perspective* (eds Barton, L. et al.) 309–324 (Springer, Dordrecht, 2010).

4. Bekker, A. *et al.* Iron Formations: Their origins and implications for ancient seawater chemistry. *Treatise Geochem. Second Ed.* **9**, 561–628 (2013).
5. Klein, C. Some Precambrian banded iron-formations (BIFs) from around the world: Their age, geologic setting, mineralogy, metamorphism, geochemistry, and origin. *Am. Mineral.* **90**, 1473–1499 (2005).
6. Krapež, B., Barley, M. E. & Pickard, A. L. Hydrothermal and resedimented origins of the precursor sediments to banded iron formation: Sedimentological evidence from the Early Palaeoproterozoic Brockman Supersequence of Western Australia. *Sedimentology* **50**, 979–1011 (2003).
7. Simonson, B. M. Origin and evolution of large Precambrian iron formations. *Spec. Pap. Geol. Soc. Am.* **370**, 231–244 (2003).
8. Jiang, C. Z. & Tosca, N. J. Fe(II)-carbonate precipitation kinetics and the chemistry of anoxic ferruginous seawater. *Earth Planet. Sci. Lett.* **506**, 231–242 (2019).
9. Konhauser, K. O., Kappler, A. & Roden, E. E. Iron in microbial metabolisms. *Elements* **7**, 89–93 (2011).
10. Thompson, K. J. *et al.* Photoferrotrophy, deposition of banded iron formations, and methane production in Archean oceans. *Sci. Adv.* **5**, 2869. <https://doi.org/10.1126/sciadv.aav2869> (2019).
11. Meister, P. *et al.* Early diagenetic quartz formation at a deep iron oxidation front in the Eastern Equatorial Pacific. *Geochim. Cosmochim. Acta* **137**, 188–207 (2014).
12. Balashova, V. V. & Zavarzin, G. A. Anaerobic reduction of ferric iron by hydrogen bacteria. *Mikrobiologiya* **48**, 773–778 (1979).
13. Lovley, D. R. & Phillips, E. J. P. Organic matter mineralization with reduction of ferric iron in anaerobic sediments. *Appl. Environ. Microbiol.* **51**, 683–689 (1986).
14. Lovley, D. R., Holmes, D. E. & Nevin, K. P. Dissimilatory Fe(III) and Mn(IV) reduction. *Adv. Microb. Physiol.* **49**, 219–286 (2004).
15. Slobodkin, A. I. Thermophilic microbial metal reduction. *Mikrobiologiya* **74**, 581–595 (2005).
16. Roh, Y. *et al.* Metal reduction and iron biomineralization by a psychrotolerant Fe(III)-reducing bacterium, *Shewanella* sp. strain PV-4. *Appl. Environ. Microbiol.* **72**, 3236–3244 (2006).
17. Zavarzina, D. G. *et al.* Oxidative biotransformation of biotite and glauconite by alkaliphilic anaerobes: The effect of Fe oxidation on the weathering of phyllosilicates. *Chem. Geol.* **439**, 98–109 (2016).
18. Johnson, D. B., Kanao, T. & Hedrich, S. Redox transformations of iron at extremely low pH: Fundamental and applied aspects. *Front. Microbiol.* **3**, 96. <https://doi.org/10.3389/fmicb.2012.00096> (2012).
19. Roden, E. Microbiological controls on geochemical kinetics 1: Fundamentals and case study on microbial Fe(III) oxide reduction. In *Kinetics of Water-Rock Interaction* (eds Brantley, S. *et al.*) 335–415 (Springer, New York, 2008).
20. O’Loughlin, E. J. *et al.* Effects of bound phosphate on the bioreduction of lepidocrocite (γ -FeOOH) and maghemite (γ -Fe₂O₃) and formation of secondary minerals. *Environ. Sci. Technol.* **47**, 9157–9166 (2013).
21. Pentráková, L., Su, K., Pentrák, M. & Stucki, J. W. A review of microbial redox interactions with structural Fe in clay minerals. *Clay Miner.* **48**, 543–560 (2013).
22. Liu, G. *et al.* Microbial reduction of Fe(III)-bearing clay minerals in the presence of humic acids. *Sci. Rep.* **7**, 45354. <https://doi.org/10.1038/srep45354> (2017).
23. Toshchakov, S. V. *et al.* Genomic insights into energy metabolism of *Carboxydollatherrautotrophica* coupling hydrogenogenic co-oxidation with the reduction of Fe(III) minerals. *Front. Microbiol.* **9**, 01759. <https://doi.org/10.3389/fmicb.2018.01759> (2018).
24. Widdel, F. *et al.* Ferrous iron oxidation by anoxygenic phototrophic bacteria. *Nature* **362**, 834–836 (1993).
25. Straub, K. L., Benz, M., Schink, B. & Widdel, F. Anaerobic, nitrate-dependent microbial oxidation of ferrous iron. *Appl. Environ. Microbiol.* **62**, 1458–1460 (1996).
26. Bryce, C. *et al.* Microbial anaerobic Fe(II) oxidation—ecology, mechanisms and environmental implications. *Environ. Microbiol.* **20**, 3462–3483 (2018).
27. Gracheva, M. A. *et al.* Mössbauer study of iron minerals transformations by *Fuchsiellaferrireducens*. *Hyperfine Interact.* **238**, 84. <https://doi.org/10.1007/s10751-017-1460-4> (2017).
28. Zavarzina, D. G. *et al.* Syntrophic growth of alkaliphilic anaerobes controlled by ferric and ferrous minerals transformation coupled to acetogenesis. *ISME J.* **14**, 425–436 (2020).
29. Weiss, M. *et al.* The physiology and habitat of the last universal common ancestor. *Nat. Microbiol.* **1**, 16116. <https://doi.org/10.1038/nmicrobiol.2016.116> (2016).
30. Luxsk, B. Thermophiles; or, the modern prometheus: The importance of extreme microorganisms for understanding and applying extracellular Electron TransferTable_1.docx. *Front. Microbiol.* **10**, 818 (2019).
31. Gorin, D. A. *et al.* Surface morphology and optical and magnetic properties of polyelectrolyte/magnetite nanoparticles nanofilms. *Tech. Phys.* **54**, 1675–1680 (2009).
32. Zavarzina, D. G. *et al.* Reduction of synthetic ferrihydrite by a binary anaerobic culture of *Anaerobacillusalkalilacustris* and *Geoalkalibacterferrihydriticus* grown on mannitol at pH 9.5. *Microbiology* **80**, 743–757 (2011).
33. Espitalié, J. & Bordenave, M. L. Screening techniques for source rocks evaluation; tools for source rocks routine analysis; Rock–Eval pyrolysis. In *Applied Petroleum Geochemistry* (ed. Bordenave, M. L.) 273–261 (Editions Technip, Paris, 1993).
34. Basen, M. & Müller, V. “Hot” acetogenesis. *Extremophiles* **21**, 15–26 (2017).
35. Menzel, P. *et al.* Comparative metagenomics of eight geographically remote terrestrial hot springs. *Microb. Ecol.* **70**, 411–424 (2015).
36. Slobodkin, A., Sokolova, T., Lysenko, A. & Wiegel, J. Reclassification of *Thermoterrabacteriumferrireducens* as *Carboxydotherrmusferrireducens* comb. nov., and emended description of the genus *Carboxydotherrmus*. *Int. J. Syst. Evol. Microbiol.* **56**, 2349–2351 (2006).
37. Yoneda, Y. *et al.* *Carboxydotherrmuspertinax* sp. nov., a thermophilic, hydrogenogenic, Fe(III)-reducing, sulfur-reducing carboxydotrophic bacterium from an acidic hot spring. *Int. J. Syst. Evol. Microbiol.* **62**, 1692–1697 (2012).
38. Feng, J. *et al.* Direct electron uptake from a cathode using the inward Mtr pathway in *Escherichiacoli*. *Bioelectrochemistry* **134**, 107498. <https://doi.org/10.1016/j.bioelechem.2020.107498> (2020).
39. Sekiguchi, Y. *et al.* *Thermodesulfovibrioaggregans* sp. nov. and *Thermodesulfovibriothiophilus* sp. nov., anaerobic, thermophilic, sulfate-reducing bacteria isolated from thermophilic methanogenic sludge, and emended description of the genus *Thermodesulfovibrio*. *Int. J. Syst. Evol. Microbiol.* **58**, 2541–2548 (2008).
40. Losey, N. A. *et al.* *Thermoanaerobaculumaquaticum* gen. nov., sp. nov., the first cultivated member of acidobacteria subdivision 23, isolated from a hot spring. *Int. J. Syst. Evol. Microbiol.* **63**, 4149–4157 (2013).
41. Kulichevskaya, I. S., Suzina, N. E., Rijpstra, W. I. C., Sinnighe Damsté, J. S. & Dedysh, S. N. *Paludibaculum fermentans* gen. nov., sp. nov., a facultative anaerobe capable of dissimilatory iron reduction from subdivision 3 of the Acidobacteria. *Int. J. Syst. Evol. Microbiol.* **64**, 2857–2864 (2014).
42. Shi, L., Fredrickson, J. K. & Zachara, J. M. Genomic analyses of bacterial porin-cytochrome gene clusters. *Front. Microbiol.* **5**, 657. <https://doi.org/10.3389/fmicb.2014.00657> (2014).
43. Legrand, L., Mazerolles, L. & Chaussé, A. The oxidation of carbonate green rust into ferric phases: Solid-state reaction or transformation via solution. *Geochim. Cosmochim. Acta* **68**, 3497–3507 (2004).
44. Etique, M., Jorand, F. P. A. & Ruby, C. Magnetite as a precursor for green rust through the hydrogenotrophic activity of the iron-reducing bacteria *Shewanellaputrefaciens*. *Geobiology* **14**, 237–254 (2016).
45. Usman, M. *et al.* Magnetite and Green Rust: Synthesis, properties, and environmental applications of mixed-valent iron minerals. *Chem. Rev.* **118**, 3251–3304 (2018).
46. Lyons, T., Reinhard, C. & Planavsky, N. The rise of oxygen in Earth’s early ocean and atmosphere. *Nature* **506**, 307–315 (2014).

47. Sánchez-Román, M. *et al.* Microbial mediated formation of Fe-carbonate minerals under extreme acidic conditions. *Sci. Rep.* **44**, 4767. <https://doi.org/10.1038/srep04767> (2014).
48. Chistyakova, N. I., Rusakov, V. S. & Zavarzina, D. G. Mössbauer investigation of biologically-induced mineralization processes. In *Hyperfine Interactions (C)* (eds Thomas, M. F. *et al.*) 397–400 (Springer, Dordrecht, 2002).
49. Roden, E. E. & Zachara, J. M. Microbial reduction of crystalline iron(III) oxides: Influence of oxide surface area and potential for cell growth. *Environ. Sci. Technol.* **30**, 1618–1628 (1996).
50. Catling, D. C. & Zahnle, K. J. The Archean atmosphere. *Sci. Adv.* **6**, eaax1420. <https://doi.org/10.1126/sciadv.aax1420> (2020).
51. Martin, W. F. (2020) Older than genes: The acetyl CoA pathway and origins. *Front. Microbiol.* **11**, 817. <https://doi.org/10.3389/fmicb.2020.00817> (2020).
52. Gavrillov, S. N., Lloyd, J. R., Kostrikina, N. A. & Slobodkin, A. I. Fe(III) oxide reduction by a Gram-positive thermophile: Physiological mechanisms for dissimilatory reduction of poorly crystalline Fe(III) oxide by a thermophilic Gram-positive bacterium *Carboxydotherrmusferrireducens*. *Geomicrobiol. J.* **29**, 804–819 (2012).
53. Kamnev, A. A. & Tugarova, A. V. Sample treatment in Mossbauer spectroscopy for protein-related analyses: Nondestructive possibilities to look inside metalcontaining biosystems. *Talanta* **174**, 819–837 (2017).
54. Matsnev, M. E. & Rusakov, V. S. SpectrRelax: An application for Mössbauer spectra modeling and fitting. *AIP Conf. Proc.* **1489**, 178–185 (2012).
55. Merkel, A. Y., Tarnovetskii, I. Y., Podosokorskaya, O. A. & Toshchakov, S. V. Analysis of 16S rRNA primer systems for profiling of thermophilic microbial communities. *Microbiol. (Russian Fed)* **88**, 671–680 (2019).
56. Caporaso, J. G. *et al.* QIIME allows analysis of high-throughput community sequencing data. *Nat. Methods* **7**, 335–336 (2010).
57. Quast, C. *et al.* The SILVA ribosomal RNA gene database project: Improved data processing and web-based tools. *Nucleic Acids Res.* **41**(Database issue), D590–D596. <https://doi.org/10.1093/nar/gks1219> (2013).
58. Shvarov, Y. V. HCh: New potentialities for the thermodynamic simulation of geochemical systems offered by windows. *Geochem. Int.* **46**, 834–839 (2008).
59. Shvarov, Y. A suite of programs, OptimA, OptimB, OptimC, and OptimS compatible with the Unitherm database, for deriving the thermodynamic properties of aqueous species from solubility, potentiometry and spectroscopy measurements. *Appl. Geochem.* **55**, 17–27 (2015).
60. Drissi, S. H., Refait, P., Abdelmoula, M. & Génin, J. M. R. The preparation and thermodynamic properties of Fe(II) Fe(III) hydroxide-carbonate (green rust 1); Pourbaix diagram of iron in carbonate-containing aqueous media. *Corros. Sci.* **37**, 2025–2041 (1995).

Acknowledgements

We are grateful to G. Mitenko and A.O. Alekseev for SEM/EDS analysis. The work of DZ, AM, NC, AA, MG was supported by the Russian Science Foundation, project no. 17-74-30025 (iron minerals analysis, phylogenetic analysis and publication of the manuscript). The work was supported by the Ministry of Science and Higher Education of the Russian Federation (cultivation experiments). Thermodynamic calculations were performed with the support of the RFBR research project no. 18-05-00818.

Author contributions

D.Z., E.B.-O., T.K. and S.G. convened the research; D.Z., T.K. and S.G. performed cultivation experiments, N.C., M.G., A.A., M.C., Y.K., A.B. performed mineralogical analyzes and interpreted their results; A.M. and A.P. performed 16S-based analyzes (NGS); A.B. performed thermodynamic calculations; D.Z., T.K., E.B.-O., S.G., and A.B. analyzed the data; D.Z., N.C., M.G., A.A., E.B.-O., S.G., A.M. and A.B. wrote the manuscript.

Competing interests

The authors declare no competing interests.

Additional information

Supplementary Information The online version contains supplementary material available at <https://doi.org/10.1038/s41598-020-78605-7>.

Correspondence and requests for materials should be addressed to D.G.Z.

Reprints and permissions information is available at www.nature.com/reprints.

Publisher's note Springer Nature remains neutral with regard to jurisdictional claims in published maps and institutional affiliations.



Open Access This article is licensed under a Creative Commons Attribution 4.0 International License, which permits use, sharing, adaptation, distribution and reproduction in any medium or format, as long as you give appropriate credit to the original author(s) and the source, provide a link to the Creative Commons licence, and indicate if changes were made. The images or other third party material in this article are included in the article's Creative Commons licence, unless indicated otherwise in a credit line to the material. If material is not included in the article's Creative Commons licence and your intended use is not permitted by statutory regulation or exceeds the permitted use, you will need to obtain permission directly from the copyright holder. To view a copy of this licence, visit <http://creativecommons.org/licenses/by/4.0/>.

© The Author(s) 2020